

Analyzing Gravastar Structure with the Finch-Skea Metric in Extended Modified Symmetric Teleparallel Gravity

Iqra Ibrar ^{*} and M. Sharif [†]

Department of Mathematics and Statistics, The University of Lahore,
1-KM Defence Road Lahore-54000, Pakistan.

Abstract

This study analyzes the physical features of a gravastar within the $f(\mathcal{Q}, \mathbb{T})$ gravity framework, where \mathcal{Q} is the non-metricity scalar and \mathbb{T} is the trace of the energy-momentum tensor. Gravastars present a viable alternative to black holes, featuring a central de Sitter core, a surrounding thin shell and a dynamic layer in the Schwarzschild exterior that separates these two regions. Using the Finch-Skea metric, the necessary field equations for the core and shell are derived, while the Israel junction conditions maintain a seamless connection between the inner and outer regions. This work extensively explores crucial aspects such as energy distribution, proper length, energy conditions, entropy and the equation of state parameter. The model's stability is studied through the effective potential, redshift, causality conditions and adiabatic index. Our results highlight the essential role of modified gravity in maintaining the structural viability and stability of gravastars.

Keywords: Israel formalism; $f(\mathcal{Q}, \mathbb{T})$ gravity; Gravastars.

PACS:04.70.Bw; 04.50.kd; 04.40.Dg.

^{*}iqraibrar26@gmail.com

[†]msharif.math@pu.edu.pk

1 Introduction

Astrophysical research reveals that the universe commenced its expansion approximately 13.8 billion years ago, leading to a rapid cooling of its temperature. This vigorous expansion facilitated the formation of large-scale cosmic structures, including stars, planets and galaxies, each exhibiting unique and remarkable features. Various theoretical models have been developed to explain the mechanisms behind the creation of these celestial bodies. Einstein's formulation of General Relativity (GR) fundamentally transformed our understanding of the cosmos by linking the motion of massive objects to the curvature of spacetime induced by gravitational fields. Following this, Edwin Hubble [1] observations demonstrated that galaxies are moving away from us at accelerating speeds, a phenomenon strongly supported by empirical data. The driving force behind this accelerated expansion is attributed to an elusive entity known as dark energy (DE), characterized by its significant negative pressure. Despite its success in describing cosmic acceleration, the standard cold dark matter (Λ CDM) model, which incorporates the cosmological constant (Λ) from GR, faces critical challenges. Notably, there exists a stark discrepancy of about 120 orders of magnitude between the observed value of Λ and the theoretically predicted vacuum energy density. Additionally, the model struggles to explain why the current value of Λ is comparable to the present matter density, raising questions about its completeness in describing the universe's evolution [2].

The prevailing big bang theory offers a comprehensive framework for understanding the universe's origin and its subsequent expansion from an initial singularity (a point of infinite density and temperature). However, in the earliest moments of the universe, the singularity existed in an extremely energetic regime where GR becomes ineffective due to expected quantum phenomena. This limitation has prompted the scientific community to explore alternative models to address these cosmological conundrums. One such innovative approach is the bounce theory, which proposes a cyclic model of cosmic expansion and contraction, thereby avoiding the initial singularity inherent in the big bang scenario. By positing recurrent phases of expansion and contraction, bounce theory provides a robust foundation for developing models that circumvent the singularity problem. Moreover, challenges like the flatness problem, monopole abundance and the horizon dilemma further indicate that the standard GR-based cosmological model is insufficient for explaining the universe under extreme conditions. Consequently, there is a

growing necessity for theories that integrate quantum mechanics with gravity to achieve a unified description of spacetime and gravitational interactions, paving the way for a more complete understanding of the universe fundamental nature.

In the quest to extend and refine our understanding of gravitational phenomena beyond the framework of GR, various modified theories of gravity have been proposed. Among these, symmetric teleparallel gravity (STG) presents a distinctive paradigm within the spectrum of gravitational theories, fundamentally diverging from GR by attributing gravitational interactions to the non-metricity of spacetime rather than its curvature [3]. In STG, the affine connection is meticulously chosen to be both torsion-free and curvature-free, thereby isolating non-metricity as the sole geometric entity responsible for mediating gravitational phenomena. This sophisticated framework leverages metric-affine geometry, enabling a more adaptable and versatile description of spacetime dynamics. By focusing solely on non-metricity, STG enables the formulation of modified gravitational models, such as $f(\mathcal{Q})$ gravity [4], which encompass crucial geometric properties for gravitational interactions. A lot of significant work has been done in this modified framework [5]-[12]. Alternative theories and observational constraints has been examined in [13]-[20].

Building on the foundational principles of STG, the $f(\mathcal{Q}, \mathbb{T})$ gravity theory marks a notable progression in the field of modified gravitational frameworks [21]. In this extended model, the \mathcal{Q} continues to characterize the geometric attributes of spacetime arising from the connection inability to maintain metric compatibility, while the trace of the energy-momentum tensor (EMT) introduces a direct coupling between matter and the geometric structure. By generalizing the traditional Einstein-Hilbert action to incorporate an arbitrary function $f(\mathcal{Q}, \mathbb{T})$, this theory allows for a more intricate interaction between the gravitational field and matter distribution, potentially addressing persistent cosmological and astrophysical challenges such as DE and the universe accelerated expansion. The integration of both non-metricity and the trace of EMT in $f(\mathcal{Q}, \mathbb{T})$ gravity provides novel insights into the dynamics of cosmic structures and the evolution of the universe. Furthermore, this theoretical framework opens new avenues for explaining phenomena that remain unresolved within GR, offering additional degrees of freedom through the function $f(\mathcal{Q}, \mathbb{T})$. Consequently, this theory not only deepens our understanding of gravitational interactions but also presents a versatile platform for exploring alternative models that could unify various

aspects of cosmological observations and theoretical predictions, thereby enriching our comprehension of gravity role in the fundamental constituents of the universe. This has become subject of great interest in scientific community due to its crucial implications in the field of cosmology and astrophysics [22]-[32].

This theory has drawn the attention of researchers because of its significant theoretical consequences and its vital function in clarifying various astronomical events. Arora et al. [33] examined a modified gravity model to investigate cosmic acceleration, utilizing constraints from Hubble and supernova data. Their results indicate that this model effectively tackles the DE issue and necessitates further research in cosmology. Bhattacharjee [34] investigated gravitational baryogenesis in this gravity, finding that it can significantly enhance baryon to entropy ratio. Godani and Samanta [35] explored $f(\mathcal{Q}, \mathbb{T})$ gravity through a non-linear model, deriving cosmological implications consistent with supernova data and the Λ CDM model. Agrawal et al. [36] examined an extension of STG concerning late-time cosmic acceleration. Their work derives dynamical parameters and validates non-singular matter bounce models through energy conditions and stability analysis. Shiravand et al. [37] investigated cosmological inflation within $f(\mathcal{Q}, \mathbb{T})$ gravity, deriving modified slow-roll parameters and spectral indices. Their findings demonstrate alignment with Planck 2018 observational data by appropriately constraining free parameters. Tayde et al. [38] analyzed the potential for wormholes within the framework of $f(\mathcal{Q}, \mathbb{T})$ gravity. Recently, we have presented the ghost, generalized ghost and generalized ghost pilgrim DE models within a cohesive theoretical framework [39].

The study of self-gravitating celestial bodies has garnered significant attention from researchers due to their remarkable properties and their impact on both cosmology and astrophysics. Accurate theoretical models are essential for understanding these entities, particularly in the context of stellar gravitational collapse, which results in the creation of dense, compact structures. Although such formations exhibit intriguing geometric properties, they also present a fundamental issue due to the existence of a singularity surrounded by an event horizon. To address this, Mazur and Mottola [40] proposed the gravastar as an alternative to black holes, offering a solution that eliminates the singularity issue. Gravastars feature a core of vacuum energy with negative pressure, likely associated with DE, which prevents the formation of a singularity and produces a repulsive force.

Unlike black holes, gravastars do not have an event horizon and are char-

acterized by an outer shell composed of normal matter. Although no direct observations of gravastars have been made, their unique characteristics, such as gravitational lensing and specific shadow patterns [41], could eventually lead to their detection. Gravastars also provide an alternative explanation for the gravitational waves detected by LIGO, fueling continued research interest [42]. Building on Mazur and Mottola model [43], Visser and Wiltshire [44] simplified the gravastar structure, reducing it to three layers: a de Sitter core, a Schwarzschild exterior and a thin-shell of stiff fluid in between. This refined model removes both the event horizon and de Sitter horizon, offering a non-singular alternative to black holes [45]. Furthermore, gravastars may contain exotic forms of matter like DE, allowing researchers to explore high energy physics and the behavior of matter under extreme gravitational conditions [46].

Gravastars have increasingly captured the interest of the scientific community keen to explore their unique structural characteristics. Visser and Wiltshire [47] investigated the impact of radial perturbations on gravastar stability, successfully identifying configurations that remain stable under such disturbances. Carter [48] discovered new stable spherically symmetric gravastar solutions, emphasizing different parameter ranges and their qualitative behaviors of the equation of state (EoS) parameter. Bilic et al. [49] analyzed the geometry of gravastars with substantial radii and masses, providing deeper insights into their extensive structural properties. Ghosh et al. [50] examined gravastar geometries, enabling a thorough analysis of their various characteristics. Das et al. [51] analyzed the properties of the intermediate shell of gravastars within the modified theory of gravity and illustrated some of these features using graphical methods. Shamir and Ahmad [52] investigated the structure of gravastars in $f(\mathcal{G}, \mathbb{T})$ gravity, where \mathcal{G} represents the Gauss-Bonnet term and analyzed various physical properties, suggesting that gravastars might offer stable, non-singular solutions without the presence of an event horizon. Sharif and Waseem [53] studied gravastars within the same framework using conformal motion and found that these objects do not possess singularities. Ghosh and his colleagues [54] investigated gravastar configurations by applying the Karmarkar condition to both the interior and shell layers. Bhatti et al. [55] investigated a singularity-free gravastar model within the framework of $f(\mathcal{R}, \mathcal{G})$ gravity, where \mathcal{R} is Ricci scalar and discussed its physical properties. Pradhan et al. [56] proposed gravastars as alternatives to black holes, explaining the universe accelerated expansion. This study presents a stable, singularity-free gravastar model,

emphasizing its interior, thin-shell properties and outer vacuum region based on Schwarzschild geometry. Mohanty and Sahoo [57] studied a gravastar in $f(\mathcal{Q})$ gravity using the Krori-Barua metric, focusing on field equations, physical properties and potential differences across the thin-shell.

Recent studies in various gravitational theories have significantly contributed to the understanding of gravastars, providing valuable insights into their physical characteristics and potential detection methods. Javed et al. [58] explored how electric charge impacts gravastars in this gravity. Mohanty et al. [59] studied charged gravastars, focusing on energy density, entropy and the EoS. They also discussed how future radio telescopes might detect the shadow of a gravastar, helping to differentiate it from a black hole event horizon. Odintsov and Oikonomou [60] studied static neutron stars in the context of various inflationary models, comparing them with theoretical and observational constraints. They found that all models are compatible with constraints, with maximum masses in the mass gap region and explored the potential to distinguish inflationary attractors. Teruel et al. [61] reported the first existence of gravastar configurations in $f(\mathcal{R}, \mathbb{T})$ gravity by developing the field equations and studying four models. Sharif et al. [62] presented a novel gravastar solution in non-conservative Rastall gravity, deriving singularity-free radial metric potentials and investigating various properties of the gravastar shell, concluding it as a viable alternative to black holes.

To address the limitations of the Dourah and Ray metric [63] in modeling compact astrophysical objects, researchers introduced the Finch-Skea metric as a more effective alternative. This metric is simple in mathematics and aligns with physical reality, making it easier to understand compact stars like neutron stars. The main reason for using the Finch-Skea metric is that it meets the necessary energy conditions, ensuring that the models being created are realistic. Its analytical tractability, meaning it can be solved easily, helps in accurately solving the field equations without difficulties of numerical simulations. Additionally, the Finch-Skea metric has shown compatibility with observational data, especially in reproducing the mass-radius relationships observed in neutron stars. This alignment with empirical findings increases the predictive power of the models, bridging the gap between theoretical ideas and astronomical observations. Furthermore, the Finch-Skea metric is a valuable tool for exploring extensions in modified theories of gravity. By adapting this metric within alternative frameworks, we can investigate possible deviations and assess the robustness of stellar models under different theoretical assumptions.

Several studies have successfully applied the Finch-Skea metric in various astrophysical contexts, further supporting its relevance and motivating its use in our analysis. Finch and Skea [64] refined this metric to better align with relativistic stellar models. Bhar [65] proposed an anisotropic strange star model with the Chaplygin EoS, based on the Finch-Skea ansatz, matching observational data of SAX J 1808.4-3658 and free from central singularity. Paul and Dey [66] analyzed compact stars using the Finch-Skea metric, finding isotropy in 4D but anisotropy in higher dimensions. Their study examines physical parameters and the feasibility of stellar models in varying spacetime dimensions. Banerjee et al. [67] investigated compact astrophysical objects governed by the DE EoS using the Finch-Skea metric. Their solutions are consistent with the observed maximum mass limits of compact stars, address stability concerns and provide insights into exotic astrophysical phenomena. Sharif and Naz [68] studied gravastar structures in $f(\mathcal{R}, \mathbb{T}^2)$ gravity using the Finch-Skea metric, finding singularity-free solutions with smooth matching to Schwarzschild spacetime and viable as black hole alternatives. Dayanandan et al. [69] developed a deformed Finch-Skea anisotropic solution using gravitational decoupling and tested its physical viability for neutron stars and white dwarfs, highlighting anisotropy role in preventing gravitational collapse. Mustafa et al. [70] studied anisotropic compact stars in $f(\mathcal{Q})$ gravity using the Finch-Skea metric, analyzing stability, mass-radius relations and compactness for PSR J0437-4715, finding that compactness increases with density. Shahzad et al. [71] derived a new solution in Rastall theory with a quintessence field using the Finch-Skea ansatz, validating it for five compact stars through physical and graphical analysis, fulfilling criteria for a viable stellar model. Rej et al. [72] proposed a DE stellar model using the Finch-Skea ansatz and vanishing complexity condition, demonstrating stability and compatibility with observed compact objects, predicting masses beyond the GR limit. Karmakar et al. [73] proposed a polytropic star model in 5D Einstein-Gauss-Bonnet gravity using the Finch-Skea ansatz, analyzing EXO 1785-248, and confirming the model realism through physical viability and the effects of the Gauss-Bonnet coupling constant. Das et al. [74] proposed a relativistic model of anisotropic compact stars coupled with DE using the Finch-Skea metric, analyzing PSR J0348+0432 and demonstrating that the stiffness of the EoS varies with the DE coupling parameter. These studies underscore the versatility and robustness of the Finch-Skea metric in modeling various types of compact astrophysical objects and highlight its potential for further exploration in modified gravity theories, especially for

understanding gravastar stability and structure.

In this paper, we aim to explore the geometric and physical aspects of a gravastar, focusing on its structure and behavior within the context of modified gravity theory. This study investigates the geometry of gravastars using the Finch-Skea metric within the framework of $f(\mathcal{Q}, \mathbb{T})$ gravity. The paper is organized as follows. Section **2** introduces the formulation of $f(\mathcal{Q}, \mathbb{T})$ gravity, followed by the derivation of field equations for a spherically symmetric spacetime using the Finch-Skea metric. Section **3** explores the configuration of gravastars. In section **4**, we provide the necessary junction conditions for smoothly connecting the inner and outer regions of the gravastar. Section **5** describes several important properties of the model in the context of $f(\mathcal{Q}, \mathbb{T})$ gravity. Finally, the entire analysis is summarized in the concluding section.

2 Basic Concepts of $f(\mathcal{Q}, \mathbb{T})$ Gravity

The following discussion outlines the core principles of the $f(\mathcal{Q}, \mathbb{T})$ theory. In GR, the Levi-Civita connection serves as the foundation [75], being both torsion-free and compatible with the metric. This connection is derived from the metric itself and its first derivatives. By easing this constraint, we can define two separate rank-3 tensors: one linked to the antisymmetric component of $\hat{\Gamma}_{[\gamma\eta]}^\alpha$ and the other related to the covariant derivative of the metric tensor

$$T_{\gamma\eta}^\alpha = 2\hat{\Gamma}_{[\gamma\eta]}^\alpha, \quad \nabla_\sigma g_{\gamma\eta} \neq 0 = \mathcal{Q}_{\gamma\eta\sigma}, \quad (1)$$

the most comprehensive connection, encompassing all possible contributions, is represented as follows

$$\hat{\Gamma}_{\gamma\eta}^\varphi = \mathcal{L}_{\gamma\eta}^\varphi + \mathcal{C}_{\gamma\eta}^\varphi + \Gamma_{\gamma\eta}^\varphi. \quad (2)$$

Within this framework, $\mathcal{L}_{\gamma\eta}^\varphi$ denotes the disformation tensor, $\mathcal{C}_{\gamma\eta}^\varphi$ signifies the contortion tensor and the Levi-Civita connection is indicated by $\Gamma_{\gamma\eta}^\varphi$, which can be expressed as follows [76]

$$\mathcal{L}_{\gamma\eta}^\varphi = \frac{1}{2}g^{\varphi\sigma}(\mathcal{Q}_{\gamma\eta\sigma} + \mathcal{Q}_{\eta\gamma\sigma} - \mathcal{Q}_{\varphi\gamma\eta}), \quad (3)$$

$$\mathcal{C}_{\gamma\eta}^\varphi = \hat{\Gamma}_{[\gamma\eta]}^\varphi + g^{\varphi\sigma}g_{\gamma\vartheta}\hat{\Gamma}_{[\eta\sigma]}^\vartheta + g^{\varphi\sigma}g_{\eta\vartheta}\hat{\Gamma}_{[\gamma\sigma]}^\vartheta, \quad (4)$$

$$\Gamma_{\gamma\eta}^\varphi = \frac{1}{2}g^{\varphi\sigma}(g_{\sigma\eta,\gamma} + g_{\sigma\gamma,\eta} - g_{\gamma\eta,\sigma}). \quad (5)$$

Consequently, the \mathcal{Q} tensor can also be derived as

$$\mathcal{Q}_{\varphi\gamma\eta} = -g_{\gamma\eta,\varphi} + g_{\eta\sigma}\hat{\Gamma}_{\gamma\varphi}^{\sigma} + g_{\sigma\gamma}\hat{\Gamma}_{\eta\varphi}^{\sigma}. \quad (6)$$

In the absence of torsion, Weyl-Cartan geometry simplifies to Weyl geometry, where the connection is determined by the metric and non-metricity. In this particular situation, the contortion tensor disappears, meaning the connection is solely determined by the non-metricity tensor [77]. For symmetric connections, the Levi-Civita connection can be articulated in terms of the disformation tensor as follows

$$\Gamma_{\gamma\eta}^{\varphi} = -\mathcal{L}_{\gamma\eta}^{\varphi}. \quad (7)$$

Gravitational effects are described in the following non-covariant formulation [78]

$$\mathcal{S} = \frac{1}{16\pi} \int g^{\gamma\eta}(\Gamma_{\sigma\gamma}^{\varsigma}\Gamma_{\eta\varsigma}^{\sigma} - \Gamma_{\sigma\varsigma}^{\varsigma}\Gamma_{\gamma\eta}^{\sigma})\sqrt{-g}d^4x. \quad (8)$$

Applying Eq.(7), the action is represented as follows

$$\mathcal{S} = -\frac{1}{16\pi} \int g^{\gamma\eta}(\mathcal{L}_{\sigma\gamma}^{\varsigma}\mathcal{L}_{\eta\varsigma}^{\sigma} - \mathcal{L}_{\sigma\varsigma}^{\varsigma}\mathcal{L}_{\gamma\eta}^{\sigma})\sqrt{-g}d^4x. \quad (9)$$

Another representation of this action is

$$\mathcal{S} = \frac{1}{16\pi} \int \mathcal{Q}\sqrt{-g}d^4x, \quad (10)$$

where

$$\mathcal{Q} = -g^{\gamma\eta}(\mathcal{L}_{\sigma\gamma}^{\varsigma}\mathcal{L}_{\eta\varsigma}^{\sigma} - \mathcal{L}_{\sigma\varsigma}^{\varsigma}\mathcal{L}_{\gamma\eta}^{\sigma}). \quad (11)$$

Lets now extend STG by introducing an arbitrary function of \mathcal{Q} . In this extended framework, the Einstein-Hilbert action is modified as follows

$$\mathcal{S} = \frac{1}{16\pi} \int (\sqrt{-g}f(\mathcal{Q}) + L_m)d^4x, \quad (12)$$

where, L_m represents the matter Lagrangian, which results in the $f(\mathcal{Q})$ theory. This theory leads to the $f(\mathcal{Q}, \mathbb{T})$ framework when combined with the trace of the EMT. The action is expressed as

$$\mathcal{S} = \frac{1}{16\pi} \int \sqrt{-g}f(\mathcal{Q}, \mathbb{T})d^4x + \int \sqrt{-g}L_md^4x. \quad (13)$$

The following expressions provide the traces of the non-metricity tensor

$$\mathcal{Q}_\gamma = \mathcal{Q}_\gamma{}^\varphi{}_\varphi, \quad \tilde{\mathcal{Q}}_\gamma = \mathcal{Q}^\varphi{}_{\gamma\varphi}. \quad (14)$$

The superpotential related to \mathcal{Q} can be written as follows

$$\mathcal{P}^\gamma{}_{\phi\hbar} = -\frac{1}{2}\mathcal{L}^\gamma{}_{\phi\hbar} + \frac{1}{4}(\mathcal{Q}^\gamma - \tilde{\mathcal{Q}}_\gamma)g_{\phi\hbar} - \frac{1}{4}\delta^\gamma{}_{(\phi}\mathcal{Q}_{\hbar)}. \quad (15)$$

This yields the relationship for \mathcal{Q} as follows [79]

$$\mathcal{Q} = -\mathcal{Q}_{\gamma\phi\hbar}\mathcal{P}^{\gamma\phi\hbar} = -\frac{1}{4}\left[-\mathcal{Q}^{\gamma\phi\hbar}\mathcal{Q}_{\gamma\phi\hbar} + 2\mathcal{Q}^{\gamma\phi\hbar}\mathcal{Q}_{\hbar\gamma\phi} - 2\mathcal{Q}^\varphi\tilde{\mathcal{Q}}_\varphi + \mathcal{Q}^\varphi\mathcal{Q}_\varphi\right]. \quad (16)$$

The field equations lead to the following formulations

$$\begin{aligned} \mathbb{T}_{\gamma\eta} &= -\frac{1}{2}f(\mathcal{Q}, \mathbb{T})g_{\gamma\eta} - \frac{2}{\sqrt{-g}}\nabla^\phi(f_\mathcal{Q}\sqrt{-g}\mathcal{P}_{\phi\gamma\eta}) - f_\mathcal{Q}(\mathcal{P}_{\phi\gamma\hbar}\mathcal{Q}_\eta{}^{\phi\hbar} \\ &\quad - 2\mathcal{Q}^{\phi\hbar}{}_\gamma\mathcal{P}_{\phi\hbar\eta}) + f_\mathbb{T}(\mathbb{T}_{\gamma\eta} + \theta_{\gamma\eta}), \end{aligned} \quad (17)$$

where $f_\mathcal{Q} = \frac{\partial f}{\partial \mathcal{Q}}$ and $f_\mathbb{T} = \frac{\partial f}{\partial \mathbb{T}}$. The variation $\delta\mathbb{T} = \delta(\mathbb{T}_{\gamma\eta}g^{\gamma\eta}) = (\mathbb{T}_{\gamma\eta} + \theta_{\gamma\eta})\delta g^{\gamma\eta}$ is used.

We will now examine the spherically symmetric metric for a general space-time. In spherical coordinates, the metric is expressed in the following standard form

$$ds^2 = -e^{\alpha(r)}dt^2 + e^{\beta(r)}dr^2 + r^2(d\theta^2 + \sin^2\theta d\phi^2). \quad (18)$$

To describe the fluid distribution, we consider the anisotropic EMT as

$$\mathbb{T}_{\gamma\eta} = (\varrho + p_t)u_\gamma u_\eta + p_t g_{\gamma\eta} + (p_r - p_t)v_\gamma v_\eta, \quad (19)$$

where ϱ is the energy density, p_r and p_t represent the radial and tangential pressures, respectively. In this framework, the four-velocity components satisfy $u^\gamma u_\gamma = -1$, while the unit radial four-vector satisfies $v^\gamma v_\gamma = 1$. In $f(\mathcal{Q}, \mathbb{T})$ gravity, the field equations are expressed as [80]-[86]

$$\begin{aligned} \varrho &= -f_\mathcal{Q}\left(\mathcal{Q}(r) + \frac{1}{r^2} + \frac{(\alpha'(r) + \beta'(r))e^{-\beta(r)}}{r}\right) + \frac{2f_{\mathcal{Q}\mathcal{Q}}\mathcal{Q}'(r)e^{-\beta(r)}}{r} \\ &\quad - \frac{1}{3}f_\mathbb{T}(p_r + 2p_t + 3\varrho) + \frac{f}{2}, \end{aligned} \quad (20)$$

$$p_r = f_{\mathcal{Q}}\left(\mathcal{Q}(r) + \frac{1}{r^2}\right) + \frac{2}{3}f_{\mathbb{T}}(p_t - p_r) - \frac{f}{2}, \quad (21)$$

$$p_t = f_{\mathcal{Q}}\left[\frac{\mathcal{Q}(r)}{2} - e^{-\beta(r)}\left(\frac{\alpha''(r)}{2} + \left(\frac{\alpha'(r)}{4} + \frac{1}{2r}\right)(\alpha'(r) - \beta'(r))\right)\right] - f_{\mathcal{Q}\mathcal{Q}}e^{-\beta(r)}\mathcal{Q}'(r)\left(\frac{\alpha'(r)}{2} + \frac{1}{r}\right) + \frac{1}{3}f_{\mathbb{T}}(p_r - p_t) - \frac{f}{2}. \quad (22)$$

Additionally, \mathcal{Q} can be represented as follows [57]

$$\mathcal{Q}(r) = \frac{2e^{-\beta(r)}}{r}\left(\frac{1}{r} + \alpha'(r)\right). \quad (23)$$

Here, the prime symbol signifies differentiation with respect to r . We employ a specific model for $f(\mathcal{Q}, \mathbb{T})$, expressed as [87]

$$f(\mathcal{Q}, \mathbb{T}) = \mu\mathcal{Q} + \nu\mathbb{T}, \quad (24)$$

where, μ and ν are arbitrary non-zero constants. This cosmological model is extensively reviewed in the current literature [88]. Substituting Eqs.(23) and (24) into Eqs.(20) through (22), we obtain

$$\varrho = \frac{1}{36(\nu + 1)r^2}\{\mu e^{-\beta(r)}(r(2(2\nu - 3)r\alpha''(r) - (2\nu - 3)\alpha'(r)(r\beta'(r) - 4) + (2\nu - 3)r\alpha'(r)^2 - 4(\eta + 6)\beta'(r)) - 4(\nu a + 6)(e^{\beta(r)} - 1))\}, \quad (25)$$

$$p_r = \frac{1}{36(\nu + 1)r^2}\{\mu e^{-\beta(r)}(4(\nu + 6)(e^{\beta(r)} - 1) - r(2(2\nu - 3)r\alpha''(r) + \alpha'(r) \times (8(\nu + 3) + (3 - 2\nu)r\beta'(r)) + (2\nu - 3)r\alpha'(r)^2 - 4(\nu - 3)\beta'(r)))\}, \quad (26)$$

$$p_t = \frac{1}{18(\nu + 1)r^2}\{\mu e^{-\beta(r)}(r(-2(\nu + 3)r\alpha''(r) + \alpha'(r)(-4\nu + (\nu + 3)r\beta'(r) - 3) + (\nu + 3)(-r)\alpha'(r)^2 + (2\nu + 3)\beta'(r)) + 2(\nu - 3)(e^{\beta(r)} - 1))\}. \quad (27)$$

We utilize the Finch-Skea solution because it provides a simple and efficient model for obtaining viable outcomes for the interior spacetime. This is due to its well-behaved nature and its ability to satisfy all criteria for physical acceptability, as confirmed by Delgaty and Lake [89]. Over the time, the Finch-Skea isotropic stellar model has been extensively generalized by various researchers to study a wide range of stellar objects. Additionally,

the Finch-Skea ansatz has been applied to interpret astrophysical systems within different gravitational frameworks. In our current model, the Finch-Skea ansatz and its solution play a central role. Specifically, the form of e^β has been directly adopted from the Finch-Skea solution [64]. However, the expression for e^α includes modifications that were introduced in prior studies [90] and are aligned with the framework of the Finch-Skea metric used in this work. These modifications were necessary to adapt the solution to the physical conditions and requirements of the modified gravitational theory employed in this study. Its regularity at the center and smooth matching between interior and exterior regions make it ideal for analyzing compact objects like gravastars. This solution is particularly useful in studying the physical and geometric properties of gravastars within the framework of modified gravity theories. These solutions are formulated as [90]

$$e^{\alpha(r)} = \left(\xi + \frac{1}{2} r \varphi \sqrt{r^2 \chi} \right)^2, \quad e^{\beta(r)} = r^2 \chi + 1. \quad (28)$$

Here, ξ , φ and χ are non-zero constants that can be determined through matching conditions. By applying Eq.(28) into Eqs.(25) through (27), we obtain the corresponding equations

$$\begin{aligned} \varrho = & -\{\mu\chi((\nu+6)r^5\varphi\chi^2 - 5(\nu-6)r^3\varphi\chi + 2(\eta+6)\xi(r^2\chi)^{3/2} + 6(\eta+6) \\ & \times \xi\sqrt{r^2\chi} + 6(3-2\nu)r\varphi)\}\{9(\nu+1)(r^2\chi+1)^2(r^3\varphi\chi + 2\xi\sqrt{r^2\chi})\}^{-1}, \end{aligned} \quad (29)$$

$$\begin{aligned} p_r = & \{\mu\chi((\nu+6)r^5\varphi\chi^2 - (5\nu+24)r^3\varphi\chi + 2(\nu+6)\xi(r^2\chi)^{3/2} + 6\nu\xi\sqrt{r^2\chi} \\ & - 6(2\nu+3)r\varphi)\}\{9(\nu+1)(r^2\chi+1)^2(r^3\varphi\chi + 2\xi\sqrt{r^2\chi})\}^{-1}, \end{aligned} \quad (30)$$

$$\begin{aligned} p_t = & \{\mu\chi((\nu-3)r^5\varphi\chi^2 - (5\nu+6)r^3\varphi\chi + 2(\nu-3)\xi(r^2\chi)^{3/2} + 6\nu\xi\sqrt{r^2\chi} \\ & - 6(2\nu+3)r\varphi)\}\{9(\nu+1)(r^2\chi+1)^2(r^3\varphi\chi + 2\xi\sqrt{r^2\chi})\}^{-1}. \end{aligned} \quad (31)$$

Anisotropic (Δ) pressure refers to the condition where the pressure within a material or system is not uniform in all directions. This directional dependence of pressure can significantly influence the behavior and stability of physical systems, such as stars, where anisotropic pressure can affect their structural integrity and evolution [91]. Figure 1 shows that p_r exceeds p_t in the current model, leading to negative anisotropy and an inward directed attractive force. Let us consider p_r and p_t as p . Adding Eqs.(30) and (31),

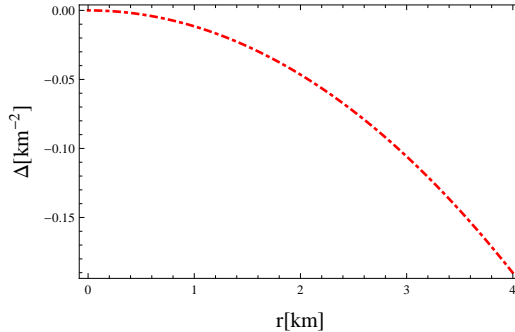


Figure 1: Plot of Δ against r .

it follows that

$$p = \{\mu\chi((2\nu + 3)r^5\varphi\chi^2 - 10(\nu + 3)r^3\varphi\chi + 2(2\nu + 3)\xi(r^2\chi)^{3/2} + 12\nu\xi \times \sqrt{r^2\chi} - (\nu + 3)r\varphi)\}\{9(\nu + 1)(r^2\chi + 1)^2(r^3\varphi\chi + 2\xi\sqrt{r^2\chi})\}^{-1}. \quad (32)$$

For mathematical analysis, treating p_r and p_t as a single p makes the equations more manageable. This approach helps to simplify the calculation of essential properties like stability and entropy without compromising the gravastar core physical characteristics.

3 Gravastar Structure and Configuration

In this section, we analyze the gravastar, focusing on three distinct regions.

- The core region, where the equation $p = -\rho$ applies.
- The thin-shell region, where the relationship $p = \rho$ is valid.
- The outer region, where $p = 0$ is applicable.

3.1 Inner Region

The key parameter in the cosmic EoS is expressed as $\omega = \frac{p}{\rho}$, where ω is a variable applied across the three distinct regions in the Mazur and Motola model [40]. In this scenario, we explore an intriguing gravitational source in the inner region. Although dark matter and DE are commonly regarded as

separate entities, they might actually be different manifestations of the same underlying phenomenon. Our aim is to investigate the EoS to characterize the dark sector within the inner region, as described by

$$p = -\varrho. \quad (33)$$

By substituting Eq.(33) into Eq.(29) and then combining the result with Eq.(32), we get

$$\begin{aligned} & \{\mu\chi((\nu - 3)r^5\varphi\chi^2 - 5(\nu + 12)r^3\varphi\chi + 2(\nu - 3)\xi(r^2\chi)^{3/2} + 6(\nu - 6)\xi\sqrt{r^2\chi} \\ & - 6(2\nu + 9)r\varphi)\}\{(\nu + 1)(r^2\chi + 1)(r^3\varphi\chi + 2\xi\sqrt{r^2\chi})\}^{-1} = 0. \end{aligned} \quad (34)$$

The active gravitational mass $\mathbf{M}(r)$ is determined as [92]

$$\mathbf{M}(r) = 4\pi \int_0^r \zeta^2 \varrho(\zeta) d\zeta.$$

Using Eq.(29), the result is given as follows

$$\begin{aligned} \mathbf{M} &= 4\pi \int \{r^2(-(\mu\chi((\nu + 6)r^5\varphi\chi^2 - 5(\nu - 6)r^3\varphi\chi + 2(\nu + 6) \\ & \times \xi(r^2\chi)^{3/2} + 6(\eta + 6)\xi\sqrt{r^2\chi} + 6(3 - 2\nu)r\varphi)))\}\{9(\nu + 1)(r^2\chi + 1)^2 \\ & \times (r^3\varphi\chi + 2\xi\sqrt{r^2\chi})\}^{-1} dr. \end{aligned}$$

In Figure 2, the numerical solution to this equation is shown, confirming the model dependability. The graph reveals a continuous increase in mass as radius grows, which aligns with the physical principle that mass should always rise as a function.

3.2 Shell

Here, we analyze a stiff perfect fluid governed by the EoS defined as

$$p = \varrho. \quad (35)$$

This fluid is confined within a thin-shell. The EoS used here is a specific form of a barotropic EoS, defined by $\omega = 1$, which leads to the relation $p = \omega\varrho$. In barotropic fluids, pressure depends solely on density, expressed as $p = p(\varrho)$, indicating a direct interdependence between pressure and density. Although

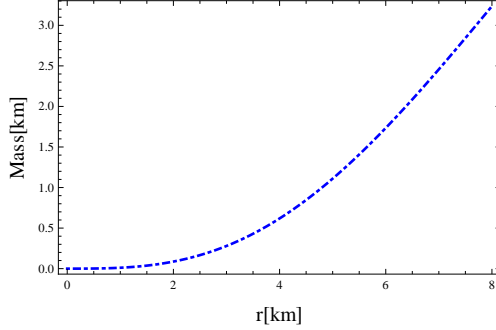


Figure 2: Plot of M with respect to r .

these types of fluids are often considered improbable, they provide an essential educational resource by demonstrating various techniques for investigating different systems and addressing physically interesting challenges. In this context, Zel'dovich [93] was the first to introduce the idea of this fluid, characterizing it as a stiff fluid. Staelens et al. [94] conducted an in-depth analysis of the gravitational collapse of an over-dense barotropic fluid governed by a linear EoS within a cosmological framework. This paradigm has been extensively adopted by the astrophysical and cosmological research communities [95]. Solving the field equations in non-vacuum regions, such as boundary layers, inherently presents significant computational challenges. Nevertheless, an analytical solution was successfully derived under the thin-shell approximation, specifically under the condition that $e^{-\beta(r)}$ remains positive and markedly smaller than unity. Building upon Israel conjecture [96], we posit that the intermediary region separating the two spacetime manifolds must constitute a thin-shell. Furthermore, as the radial coordinate r approaches zero, any parameter dependent on r can generally be considered negligible (i.e., substantially less than one). This approximation facilitates the simplification of our field equations from Eqs.(20)-(22) to the following

$$\varrho + \frac{\nu}{2}(5p + \varrho) = \mu \left(\frac{e^{-\beta(r)}\beta'(r)}{r} + \frac{1}{r^2} \right), \quad (36)$$

$$p + \frac{\nu}{2}(\varrho - 3p) = \mu \left(-\frac{1}{r^2} \right), \quad (37)$$

$$p + \frac{\nu}{2}(\varrho - 3p) = -\mu \left(\beta'(r)\alpha'(r)\frac{e^{-\beta(r)}}{4} + \frac{e^{-\beta(r)}\beta'(r)}{2r} \right). \quad (38)$$

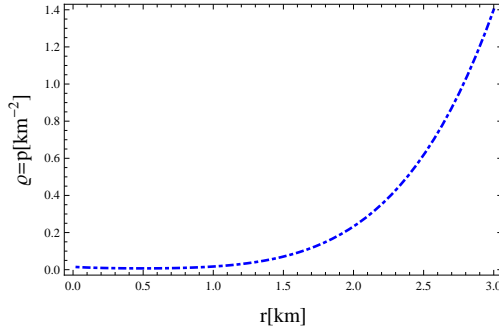


Figure 3: Plot of $\rho = p$ with respect to r .

Substituting Eqs.(23), (24), (28) and (35) into Eqs.(36) through (38), we first combine Eqs.(36) and (37), and then add Eqs.(37) and (38). Solving the resulting pair of equations leads us to the final outcome

$$e^{-\beta(r)} = -c_1 - \frac{(\nu + 2)(r^2\chi + 1)(2\xi + r\varphi\sqrt{r^2\chi})}{r^2\chi(6(\nu - 2)\xi + (\nu - 10)r\varphi\sqrt{r^2\chi})}, \quad (39)$$

where c_1 is the constant of integration. Figure **3** depicts the variations in p and ρ . It is evident that ρ within the shell steadily rises as it approaches the outer boundary. Composed of a stiff fluid, the shell demonstrates that both p and ρ increase uniformly towards the outer surface. This indicates that the concentration of stiff matter is greater at the outer edge than in the shell inner region.

3.3 Exterior Region

The gravastar exterior conforms to the EoS $p = 0$, implying that the outer layer is completely surrounded by a vacuum. Among the most intriguing solutions to the Einstein field equations in GR is the Schwarzschild solution, which describes a spherically symmetric, static vacuum. The line element of the Schwarzschild metric can be expressed as follows

$$ds_+^2 = -\left(1 - \frac{2M}{r}\right) dt^2 + \left(1 - \frac{2M}{r}\right)^{-1} dr^2 + r^2(d\theta^2 + \sin^2\theta d\phi^2). \quad (40)$$

In this context, the symbol + denotes the exterior solution. A black hole with an isolated mass M , represented by the static spherically symmetric line element (40), is called a Schwarzschild black hole.

4 Boundary and Junction Conditions

In this section, we synchronize the internal spacetime with the external spacetime to determine the constants χ , ξ and φ . By ensuring the continuity of the metric coefficients g_{tt} , g_{rr} and $\frac{\partial g_{tt}}{\partial r}$, we establish a seamless connection between the interior and exterior regions at the boundary surface $r = R$. This matching procedure is crucial for maintaining the smoothness and consistency of the spacetime geometry at the interface between the two domains. We proceed by calculating the values of χ , ξ and φ specifically for the Schwarzschild black hole configuration. In this process, we juxtapose the temporal and radial metric coefficients from Eqs.(18) and (40). Applying Eq.(28), we ascertain that

$$1 - \frac{2M}{R} = \left(\xi + \frac{1}{2}R\varphi\sqrt{R^2\chi} \right)^2, \quad (41)$$

$$\left(1 - \frac{2M}{R} \right)^{-1} = R^2\chi + 1. \quad (42)$$

Differentiating Eq.(41) with respect to R , we have

$$\frac{2M}{R^2} = \varphi \left(R^3\varphi\chi + 2\xi\sqrt{R^2\chi} \right). \quad (43)$$

The constants χ , ξ and φ are expressed in terms of M and R through Eqs.(41)-(43). Applying these equations, we determine the following values

$$\chi = \frac{2M}{R^2(R - 2M)}, \quad (44)$$

$$\xi = \pm \frac{\sqrt{\frac{M}{R-2M}}(2R - 5M)}{2\sqrt{M}\sqrt{R}}, \quad (45)$$

$$\varphi = \pm \frac{\sqrt{M}}{\sqrt{2}R^{3/2}}. \quad (46)$$

During the derivation, we accounted for both the positive and negative branches of ξ and φ arising from the square root. To ensure the model physical viability and consistency, we select the positive branch, aligning with established practices in the literature, where only positive values are considered to maintain plausibility.

$$\chi = \frac{2M}{R^2(R-2M)}, \quad (47)$$

$$\xi = \frac{\sqrt{\frac{M}{R-2M}}(2R-5M)}{2\sqrt{M}\sqrt{R}}, \quad (48)$$

$$\varphi = \frac{\sqrt{M}}{\sqrt{2}R^{3/2}}. \quad (49)$$

The exploration of junction conditions, which govern the seamless integration between two distinct regions such as a star interior and exterior, was initiated by Sen [97]. These conditions are essential for ensuring smooth transitions across different spacetime domains. The Darmois junction conditions [98] facilitate this seamless connection by enforcing two main criteria: the interface surface must preserve the same geometry and dimensions on both sides (metric continuity), and the curvature of this surface must remain consistent across both regions (extrinsic curvature continuity). In contrast, the Israel junction conditions [96] are applicable when a thin layer, like a membrane, exists at the boundary, carrying its own energy and pressure. In such cases, the Israel conditions permit a sudden change in surface curvature across the layer, reflecting the unique properties of the thin boundary. In this work, we employ the Israel junction conditions [99] due to their effectiveness in scenarios involving a boundary between two distinct spacetime regions separated by a thin-shell of matter or energy. This methodology is especially suitable for examining surface layers that carry mass. While the metric coefficients remain continuous across the boundary, their derivatives may show discontinuities at the hypersurface, which is consistent with the requirements for analyzing such thin-shells.

The metric induced on the boundary is represented by the following line element

$$ds^2 = -d\tau^2 + R(\tau)^2 d\theta^2 + R(\tau)^2 \sin^2 \theta d\phi^2. \quad (50)$$

Here, τ represents the proper time. To maintain the stability of the thin-shell, it is necessary to apply the Lanczos equations to determine the surface

tension and pressure [100]

$$S_j^i = -\frac{1}{8\pi}\{[A_j^i] - \delta_j^i A\}, \quad (51)$$

where $[A_j^i] = A_j^{+i} - A_j^{-i}$, $A = \text{tr}[A_{ij}] = [A_j^j]$ and the indices i and j correspond to the coordinates on the hypersurface ($i, j = 0, 2, 3$). The extrinsic curvature is defined as follows

$$A_{ij}^\pm = -n_v^\pm \left(\frac{d^2 x_\pm^v}{d\phi^i d\phi^j} + \Gamma_{lm}^v \frac{dx_\pm^l}{d\phi^i} \times \frac{dx_\pm^m}{d\phi^j} \right), \quad l, m = 0, 1, 2, 3. \quad (52)$$

Here, ϕ^i represents the intrinsic coordinates and the components of $A_j^{i\pm}$ are defined as follows

$$A_\tau^{\tau\pm} = \frac{\Pi' + 2\ddot{R}}{\sqrt{\Pi_\pm(R) + \dot{R}^2}}, \quad A_\theta^{\theta\pm} = \frac{\sqrt{\Pi_\pm(R) + \dot{R}^2}}{R}, \quad A_\phi^{\phi\pm} = \sin^2 \theta A_\theta^{\theta\pm}. \quad (53)$$

The unit normals to the hypersurface n_v^\pm are expressed as follows

$$n_v^\pm = \left(\frac{\dot{R}}{\Pi_\pm(R)}, \sqrt{\Pi_\pm(R) + \dot{R}^2}, 0, 0 \right), \quad (54)$$

where \dot{R} represents derivative of R with respect to τ .

The Lanczos equations are employed to determine the surface energy density ρ and surface pressure P of thin-shell gravastars, which are defined as follows

$$\begin{aligned} \rho &= -\frac{[A_\theta^\theta]}{4\pi} = -\frac{1}{4\pi R} \left(\sqrt{\dot{R}^2 + \Pi_+(R)} - \sqrt{\dot{R}^2 + \Pi_-(R)} \right), \quad (55) \\ P &= \frac{[A_\theta^\theta] + [A_\tau^\tau]}{8\pi} = \frac{1}{8\pi R} \left[\frac{2\dot{R}^2 + 2R\ddot{R} + 2\Pi_+(R) + R\Pi'_+(R)}{\sqrt{\dot{R}^2 + \Pi_+(R)}} \right. \\ &\quad \left. - \frac{2\dot{R}^2 + 2R\ddot{R} + 2\Pi_-(R) + R\Pi'_-(R)}{\sqrt{\dot{R}^2 + \Pi_-(R)}} \right]. \quad (56) \end{aligned}$$

When the system reaches equilibrium, with the shell remaining fixed at the throat radius $R = R_0$ (i.e., $\dot{R}_0 = 0$ and $\ddot{R}_0 = 0$), the equations reduce to the following form

$$\rho_0 = -\frac{1}{4\pi R_0} [\sqrt{\Pi_+(R_0)} - \sqrt{\Pi_-(R_0)}], \quad (57)$$

$$P_0 = -\rho_0 + \frac{1}{8\pi} \left[\frac{\Pi'_+(R_0)}{\sqrt{\Pi_+(R_0)}} - \frac{\Pi'_-(R_0)}{\sqrt{\Pi_-(R_0)}} \right]. \quad (58)$$

The exterior function is expressed as

$$\Pi_+(R_0) = 1 - \frac{2M}{R_0}. \quad (59)$$

The interior function is characterized as

$$\begin{aligned} \Pi_-(R_0) &= -c_1 - \{(\nu + 2)R_0^2(R_0 - 2M)\left(\frac{2R_0^2M}{R_0^2(R_0 - 2M)} + 1\right)(\sqrt{2}R_0\psi \\ &\times \{\{R_0^2M\}\{R_0^2(R_0 - 2M)\}^{-1}\}^{\frac{1}{2}} + \frac{\sqrt{\frac{M}{R_0 - 2M}}(2R_0 - 5M)}{\sqrt{M}\sqrt{R_0}})\}\{2R_0^2M \\ &- (\sqrt{R_0}(\nu)\psi\sqrt{\frac{R_0^2M}{R_0^2(R_0 - 2M)}} + \{(\nu - 2)\sqrt{\frac{M}{R_0 - 2M}}(R_0 - 5M)\} \\ &\times \{\sqrt{M}\sqrt{R_0}\})\}^{-1}. \end{aligned} \quad (60)$$

The dynamic behavior of a thin-shell can be analyzed through the equation of motion and the conservation principle. These equations are fundamental for determining the stable regions within a geometric configuration. The equation of motion can be derived by rearranging Eq.(55) as follows

$$\dot{R}^2 + V(R) = 0. \quad (61)$$

The effective potential, denoted by $V(R)$, can be expressed as follows [101]

$$V(R) = \frac{1}{2}(\Pi_-(R) + \Pi_+(R)) - \frac{(\Pi_-(R) - \Pi_+(R))^2}{64\pi^2 R^2 \rho^2} - 4\pi^2 R^2 \rho^2. \quad (62)$$

Next, we examine that ρ and P satisfy the conservation equation

$$\frac{d}{d\tau}(\rho 4\pi R^2) + P \frac{d4\pi R^2}{d\tau} = 0. \quad (63)$$

By utilizing this equation, we are able to determine

$$\rho' = -(\rho + P) \frac{2}{R}. \quad (64)$$

Now, we analyze the behavior of ρ_0 and P_0 at the junction surface $R = R_0$. Substituting Eqs.(59) and (60) into Eqs.(57) and (58), we obtain

$$\begin{aligned} \rho_0 &= \frac{1}{8\pi R_0} \left[2\sqrt{1 - \frac{2M}{R_0}} - \sqrt{2}(\{2\sqrt{2}R_0^{3/2}c_1(\nu - 10)M^{3/2}\psi + \sqrt{2}R_0^{5/2}(\nu + 2)\right. \\ &\times \sqrt{M}\psi + 2R_0^2(\nu + 2) + R_0M(12c_1(\nu - 2) - 5(\nu + 2)) - 30c_1(\nu - 2)M^2\} \\ &\times \left. \{M(-\sqrt{2}R_0^{3/2}(\nu - 10)\sqrt{M}\psi - 6R_0(\nu - 2) + (\nu - 2)M)\}^{-1})^{\frac{-1}{2}} \right], \quad (65) \end{aligned}$$

$$\begin{aligned} P_0 &= \frac{1}{8\pi} \left[\frac{M}{R_0^2\sqrt{1 - \frac{2M}{R_0}}} + \frac{1}{R_0} \left\{ 2\sqrt{1 - \frac{2M}{R_0}} - \sqrt{2} \{ \{ 2\sqrt{2}R_0^{3/2}c_1(\nu - 10)M^{3/2}\psi \right. \right. \\ &+ \sqrt{2}R_0^{5/2}(\nu + 2)\sqrt{M}\psi + 2R_0^2(\nu + 2) + R_0M(12c_1(\nu - 2) - 5(\nu + 2)) \\ &- 30c_1(\nu - 2)M^2 \} \{ M(-\sqrt{2}R_0^{3/2}(\nu - 10)\sqrt{M}\psi - 6R_0(\nu - 2) + 15(\nu - 2) \\ &\times M) \}^{-1} \}^{\frac{1}{2}} \} + \{ (\nu + 2)(5\sqrt{2}R_0^{3/2}(10 - 7\nu)M^{3/2}\psi + 2\sqrt{2}R_0^{5/2}(5\nu - 14) \\ &\times \sqrt{M}\psi + 2R_0^3(\nu - 10)M\psi^2 + 12R_0^2(\nu - 2) - 60R_0(\nu - 2)M + 75(\nu - 2) \\ &\times M^2) \} \{ 2\sqrt{2}M(\sqrt{2}R_0^{3/2}(\nu - 10)\sqrt{M}\psi + 6R_0(\nu - 2) - 15(\nu - 2)M)^2 \\ &\times \{ \{ 2\sqrt{2}R_0^{3/2}c_1(\nu - 10)M^{3/2}\psi + \sqrt{2}R_0^{5/2}(\nu + 2)\sqrt{M}\psi + 2R_0^2(\nu + 2) \\ &+ R_0M(12c_1(\nu - 2) - 5(\nu + 2)) - 30c_1(\nu - 2)M^2 \} \{ M(-\sqrt{2}R_0^{3/2}(\nu - 10) \\ &\times \sqrt{M}\psi - 6R_0(\nu - 2) + 15(\nu - 2)M) \}^{-1} \}^{\frac{1}{2}} \}^{-1} \right]. \quad (66) \end{aligned}$$

Figure 4 illustrates the variation of surface energy density and pressure with the thickness of thin-shell. The graph demonstrates that the energy density is positive but gradually declines from the inner boundary to the outer boundary. Meanwhile, the pressure remains negative and also decreases as it nears the outer boundary.

5 Physical Features of Gravastar

In this section, we will examine the physical properties of a gravastar, including its energy, proper length, energy conditions, entropy and the EoS parameter, at the shell equilibrium. Additionally, we will investigate the stability of the gravastar thin shell, with a focus on the effective potential, redshift, causality condition and adiabatic index.

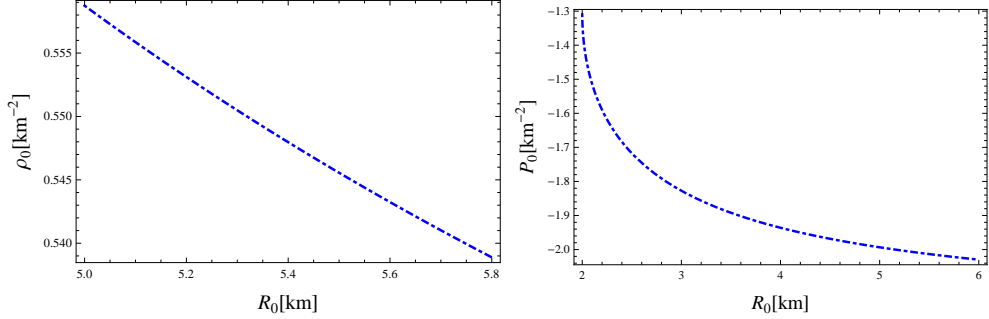


Figure 4: Plots of ρ_0 and P_0 with respect to R_0 .

5.1 Energy

The center of a gravastar indicates the existence of DE due to the negative pressure that produces a repulsive force. The energy of the shell can be determined using the following formula [102]

$$E = \int_{R_0}^{R_0+\epsilon} 4\pi R^2 \rho_0 dR. \quad (67)$$

Using Eqs.(65), we deduce that

$$\begin{aligned} E &= - \left[4\pi\zeta\chi((R_0 + \epsilon)^3 - R_0^3) ((\eta + 6)R_0^5\varphi\chi^2 - 5(\eta - 6)R_0^3\varphi\chi + 2(\eta + 6) \right. \\ &\quad \times \left. \xi(R_0^2\chi)^{3/2} + 6(\eta + 6)\xi\sqrt{R_0^2\chi} + 6(3 - 2\eta)R_0\varphi \right] \left[27(\eta + 1)(R_0^2\chi + 1) \right]^2 \\ &\quad \times \left(R_0^3\varphi\chi + 2\xi\sqrt{R_0^2\chi} \right)^{-1}. \end{aligned} \quad (68)$$

Figure 5 shows that the shell energy increases as its thickness grows.

5.2 Proper Length

According to the models proposed by Mazur and Mottola [40], the shell is positioned at the junction where two spacetimes intersect. The length of the shell spans from the outer boundary $r_2 = R_0 + \epsilon$ (ϵ denotes the thickness of the shell and a small distance), which marks the transition from the outer spacetime to the intermediate thin-shell, to the inner boundary $r_1 = R_0$,

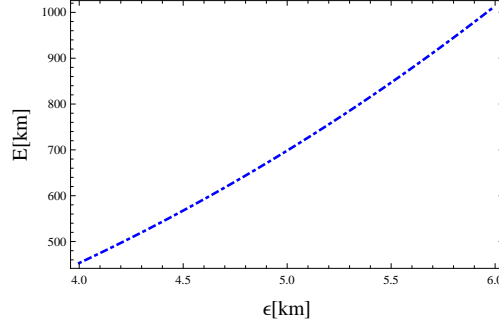


Figure 5: Plot of energy with respect to thickness.

which separates the inner region from the intermediate thin-shell. The thickness of the shell calculated between these two phase boundaries is given by [102]

$$L = \int_{R_0}^{R_0+\epsilon} \sqrt{e^{\beta(R)}} dR. \quad (69)$$

This can be converted into the interior function as

$$\begin{aligned} L = & \int_{R_0}^{R_0+\epsilon} \left[-c_1 - \left[(\nu + 2)R^2(R - 2M) \left(\frac{2R^2M}{R^2(R - 2M)} + 1 \right) (\sqrt{2}R\psi \right. \right. \\ & \times \left. \left. \{ \{ R^2M \} \{ R^2(R - 2M) \}^{-1} \}^{\frac{1}{2}} + \frac{\sqrt{\frac{M}{R-2M}}(2R - 5M)}{\sqrt{M}\sqrt{R}} \right) \right] \left[2R^2M \right. \\ & \left. \left. - \left(R(\nu)\psi \sqrt{\frac{R^2M}{R^2(R - 2M)}} + \frac{(\nu - 2)\sqrt{\frac{M}{R-2M}}(R - 5M)}{\sqrt{M}\sqrt{R}} \right) \right]^{-1} \right] dR. \quad (70) \end{aligned}$$

Using Eq.(60), we obtain

$$= \int_{R_0}^{R_0+\epsilon} \frac{1}{\Pi_-(R)} dR. \quad (71)$$

Calculating the integral in Eq.(70) proves to be quite challenging. To simplify the process, we set $\frac{d\Pi_-(R)}{dR} = \frac{1}{\Pi_-(R)}$ to solve the integral. This yields

$$L = \Pi_-(R_0 + \epsilon) - \Pi_-(R_0). \quad (72)$$

Expanding $\Pi_-(R_0 + \epsilon)$ in a Taylor series around R_0 and considering only the linear terms in ϵ . Since ϵ is very small, higher-order terms in the expansion

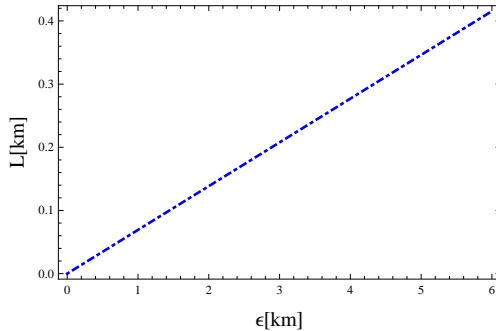


Figure 6: Plot of proper length with respect to thickness.

can be neglected. Figure 6 illustrates the relationship between proper length and shell thickness, showing that as the thickness increases, the proper length of the shell grows proportionally.

5.3 Energy Conditions

To evaluate the physical viability of geometric structures in modified theories of gravity, it is crucial to follow specific criteria known as energy conditions. These conditions act as essential guidelines to determine whether a particular arrangement of matter and energy can exist within the framework of these extended theories. By applying these criteria, we ensure that the resulting structures are consistent with our understanding of gravitational physics. The commonly recognized energy criteria are

- Null energy conditions (NEC) states that $0 \leq \rho_0 + P_0$.
- Weak energy conditions is given as $0 \leq \rho_0 + P_0$, $0 \leq \rho_0$.
- Strong energy conditions is formulated as $0 \leq \rho_0 + P_0$, $0 \leq \rho_0 + 2P_0$.
- Dominant energy conditions is given as $0 \leq \rho_0 \pm P_0$.

For the model to be considered physically viable, it must comply with these energy conditions. Our primary focus is whether the NEC is met, as this criterion signifies the existence of either ordinary or exotic matter within the thin-shell. It is crucial to emphasize that any violation of the NEC could

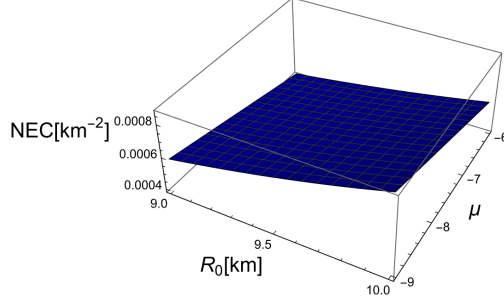


Figure 7: Plot of the NEC versus the model parameter μ .

result in the infringement of the other energy conditions. Figure 7 demonstrates that the NEC is satisfied for the given model parameter, confirming the physical viability of the model.

5.4 Entropy

According to Mazur and Mottola [40], the entropy S for the intermediate thin-shell can be calculated using the following formula

$$S = \int_{R_0}^{R_0+\epsilon} 4\pi R^2 s(R) \sqrt{e^{\beta(R)}} dR. \quad (73)$$

The entropy density $s(R)$ is defined as

$$s(R) = \frac{k^2 K_B^2 T(R)}{4\pi \hbar^2 G} = \frac{k K_B}{\hbar} \sqrt{\frac{P_0}{2\pi G}}, \quad (74)$$

where k is non-zero arbitrary constant, $T(R)$ represents the temperature, \hbar denotes Planck constant and K_B is the Boltzmann constant. In this analysis, we use geometrical units $G = 1$. Substituting this into Eq.(73), the expression for S becomes

$$S = \int_{R_0}^{R_0+\epsilon} 4\pi R^2 \frac{k K_B}{\hbar} \left(\frac{P_0}{2\pi}\right)^{\frac{1}{2}} \sqrt{e^{\beta(R)}} dR = \int_{R_0}^{R_0+\epsilon} 2\sqrt{2\pi} R^2 \frac{k K_B}{\hbar} \sqrt{P_0 e^{\beta(R)}} dR.$$

This can be simplified to

$$S = 2\sqrt{2\pi} R^2 k \frac{K_B}{\hbar} N, \quad (75)$$

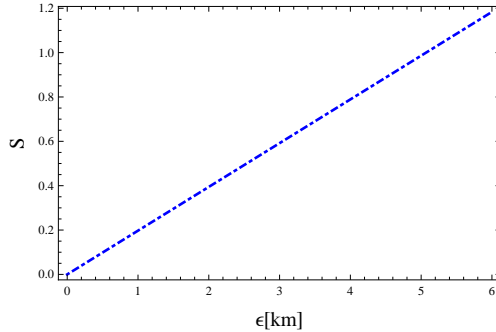


Figure 8: Plot of entropy with respect to thickness.

where

$$N = \int_{R_0}^{R_0+\epsilon} \sqrt{P_0 e^{\beta(R)}} dR = \int_{R_0}^{R_0+\epsilon} D(R) dR. \quad (76)$$

Evaluating the integral in Eq.(76) is quite complex at this stage. To simplify, let us consider $F(R)$ as the antiderivative of $D(R)$. This allows us to compute the integral using the fundamental theorem of calculus, which modifies Eq.(76) to

$$N = [F(R)]_{R_0}^{R_0+\epsilon} = F(R_0 + \epsilon) - F(R_0). \quad (77)$$

Expanding $F(R_0 + \epsilon)$ in a Taylor series around R_0 and keeping only the first-order term in ϵ , we derive from Eq.(75). However, due to the complexity of the equations, we will present only their graphical representations. Figure 8 demonstrates that as the shell thickness increases, the disorder within the gravastar rises, with entropy increasing in proportion to the shell thickness and peak at the outer surface. A shell with no thickness results in zero entropy.

5.5 The EoS Parameter

The EoS parameter, denoted as ω , is vital in cosmology and thermodynamics, relating P_0 to ρ_0 of a cosmic fluid through the equation $P_0 = \omega \rho_0$ [56]. It provides insight into the behavior of different energy forms in the universe: $\omega = 0$ corresponds to non-relativistic matter, $\omega = \frac{1}{3}$ describes radiation, and DE typically has $\omega < -\frac{1}{3}$. Observational data from cosmic microwave background radiation, galaxy clusters and supernovae suggest that DE has a value close to $\omega \approx -1$, while $\omega < -1$ corresponds to phantom energy and

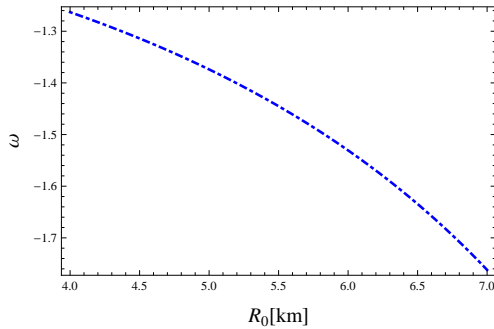


Figure 9: Plot of EoS with respect to R_0 .

$\omega \geq -1$ defines the non-phantom regime. Current research explores potential variations in the EoS parameter over time and the implications of different forms of DE, making it essential for understanding the universe fate and the evolution of its energy components. Figure 9 illustrates that ω falls below -1, entering the phantom region and highlighting the importance of the gravastar structure.

5.6 Stability Analysis

Here, we will investigate the stability of the gravastars at the shell equilibrium, with a focus on the effective potential. A positive $V''(R_0)$ indicates a stable structure, while a negative value points to instability. When $V''(R_0)$ equals to zero, the stability cannot be predicted [101]. We present only the graphical behavior of $V''(R_0)$ due to the complexity of the expressions. Figure 10 confirms that $V''(R_0) > 0$ ensuring the stable configuration of the thin-shell gravastar.

Gravitational redshift, denoted by $Z(R)$, refers to the phenomenon where light emitted from a gravitational field experiences a shift to longer wavelengths as it escapes a massive object gravitational influence. This occurs because gravity impacts the frequency of photons as light moves upwards from a gravitational well, its energy decreases, causing an increase in wavelength. The mathematical expression for gravitational redshift is given by

$$Z(R) = \frac{1}{\sqrt{-g_{tt}}} - 1.$$

Additionally, the surface redshift must remain below 2 for a stable, isotropic

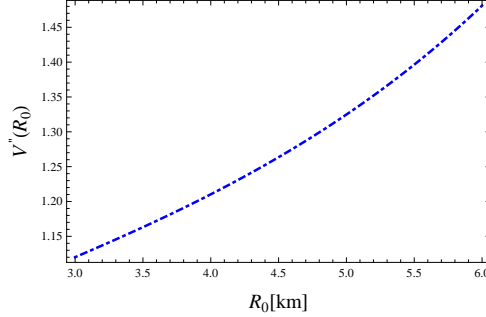


Figure 10: Plot of $V''(R_0)$ against R_0 .

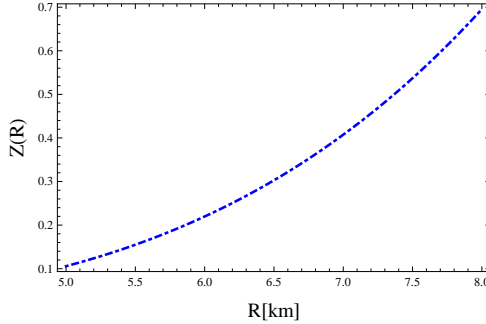


Figure 11: Plot of $Z(R)$ against R .

distribution of perfect fluid [103]. This requirement is critical for the stability of such systems, as it prevents excessive gravitational forces that could lead to instability or collapse. A surface redshift exceeding this limit suggests a gravitational field strong enough to compromise the fluid integrity, potentially leading to singularities or event horizons. Thus, ensuring the surface redshift remains within this boundary is essential for the stability and physical plausibility of perfect fluid distributions in GR. In Figure 11, the redshift parameter stays within the expected range throughout the gravastar shell, with $Z(R)$ remaining below 2. The gravitational redshift is positive and finite, steadily increasing towards the surface. This confirms the gravastar model physical stability and compatibility with the $f(\mathcal{Q}, \mathbb{T})$ framework.

We also analyze the stability by examining the causality condition and the adiabatic index. Having computed ρ and p for the thin-shell from Eq.(36)

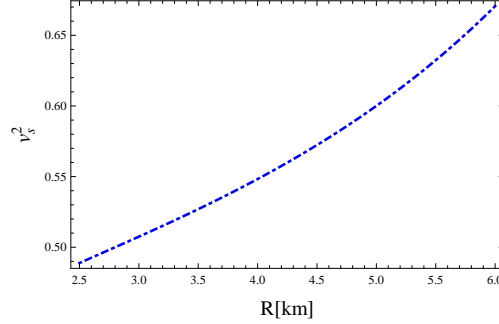


Figure 12: Plot of v_s^2 with respect to R .

and Eq.(37), we can express the speed of sound as

$$v_s^2 = \frac{p'}{\rho'}. \quad (78)$$

To determine the speed of sound specifically within the thin-shell, we evaluate this expression at R . According to Poisson and Visser [105], the causality condition dictates that the speed of sound should not exceed the speed of light (where $c = 1$ in natural units). Therefore, the speed of sound v_s^2 is anticipated to lie within the range $0 \leq v_s^2 \leq 1$. Lobo [106] applied this criterion to set a limit on wormhole stability in the presence of a cosmological constant. However, as highlighted in [105], there are limitations to using the v_s^2 as a measure of stability. Near $\omega = 1$, which corresponds to the stiff matter region, Eq.(78) may not accurately represent the v_s^2 . This is because the microscopic properties of stiff matter are not fully understood, so traditional fluid dynamics might not be applicable. Despite these limitations, the v_s^2 condition provides a necessary, though not sufficient, criterion for assessing the stability of the thin-shell around the gravastar. Substituting the necessary values into (78), we obtain v_s^2 . Figure **12** illustrates the behavior of v_s^2 with the radial distance R . The fact that the condition $0 \leq v_s^2 \leq 1$ is satisfied indicates that the gravastar maintains stability under these conditions.

The adiabatic index (Γ) is essential for evaluating the stability of stars, such as gravastars. It represents the correlation between pressure and density and how they affect a star stability. This index is calculated as

$$\Gamma = \frac{v_s^2(p + \rho)}{p}. \quad (79)$$

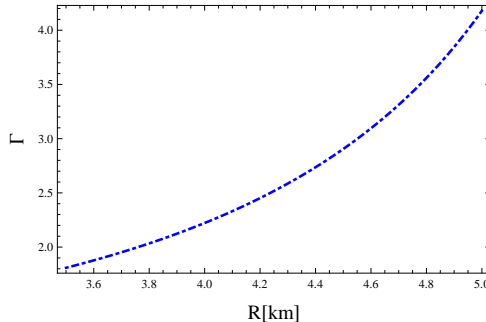


Figure 13: Plot of Γ with respect to R .

The stability of an object is determined for Γ to be greater than $4/3$. If Γ is below this critical value, the object becomes unstable and could collapse [104]. Figure **13** shows that the system meets the required stability criterion, indicating that the gravastar is both viable and stable.

6 Concluding Remarks

Gravastars have been studied under various gravitational theories. In this work, we have focused on exploring gravastars within the extended STG framework, which is effective in describing the current accelerated expansion of the universe. We have examined a gravastar solution using the Finch-Skea metric to establish a model that is both physically plausible and free of singularities, effectively circumventing the issues associated with black hole like singularities. By utilizing this metric with an ideal fluid distribution, we have studied the properties of the gravastar interior, shell and exterior regions. A summary of the results is provided as follows.

- The p_r exceeds p_t in the current model, leading to negative anisotropy and an inward directed attractive force Figure **1**.
- We have observed that as the shell radius increases, its mass also rises significantly, indicating a direct relationship between the two. This increase in mass highlights the growing influence of the shell as it expands, reflecting the model sensitivity to the physical properties of the shell (Figure **2**).

- The pressure and density in the thin-shell increase towards the outer boundary, with the outer edge becoming denser as the shell thickens. This difference in density and pressure is important for understanding the strength of the gravastar, as it shows that the outer shell is much more compressed as compared to the inner regions (Figure 3).
- We have observed that both the surface energy density and negative pressure decrease as the shell thickness increases. The surface energy density and pressure gradually diminish towards the outer boundary. This decrease indicates that as the shell expands, the energy stored per unit area is reduced, suggesting a more stable outer region (Figure 4).
- The energy inside rises as the shell thickness increases. This suggests that the energy within the shell grows in direct proportion to the radial distance. Additionally, the observed fluctuations indicate that gravastars can sustain their structural stability while steadily accumulating energy over time (Figure 5).
- The proper length of the gravastar shell increases as its thickness grows, showing a direct relationship between the two. This indicates that as the shell becomes thicker, it expands in size, with the proper length reflecting the extent of this growth (Figure 6).
- We have ensured that the NEC is satisfied for a model parameter, indicating that the gravastar shell could consist of ordinary matter. This suggests that gravastars can exist as physically plausible objects (Figure 7).
- For a stable gravastar, the entropy should reach its maximum value at the surface. We have observed that the shell entropy increases as the shell thickness expands. Our results are consistent with the previous studies [107]-[109] (Figure 8).
- The EoS parameter drops below -1, entering the phantom region. This phantom-like behavior further highlights the distinct characteristics of gravastars in this modified gravity theory (Figure 9).
- The effective potential shows that $V''(R) > 0$, meaning the thin-shell is stable (Figure 10).

- The surface redshift, causality condition and adiabatic index indicate that the gravastar satisfies the stability criteria, hence the gravastar is stable (Figures **11-13**).

In conclusion, our results present a physically plausible alternative to black holes by avoiding singularities and event horizons, although obtaining physically acceptable solutions with this specific metric potential proved more challenging than in the previous work [56]. Our model provides a more accurate analytical solution for determining the physical parameters of the shell, thereby enhancing the understanding of gravastar stability. This stability has been confirmed through different techniques. In future, exploring more general forms of $f(\mathcal{Q}, \mathbb{T})$ gravity will be crucial for deepening our understanding of gravastar solutions and assessing whether the same thickness-to-stability relationships hold across different gravity models.

In this study, we have conducted a thorough examination of the physical and stability characteristics of gravastars within the $f(\mathcal{Q}, \mathbb{T})$ gravity framework, employing the Finch-Skea metric to model their structure. By investigating properties such as energy distribution, proper length, energy conditions, entropy, and the EoS parameter, we have demonstrated the gravastar remarkable adaptability and stability. Our findings indicate that the energy inside the shell increases proportionally with its thickness, highlighting its efficient energy accumulation capability. The proper length also increases with thickness. The null energy condition is satisfied in our model, confirming its physical plausibility, while entropy increases with shell thickness. These results collectively emphasize the gravastar potential as a singularity-free alternative to black holes. Our stability analysis has revealed that the effective potential exhibits a positive second derivative, affirming the robustness of the thin shell under radial perturbations. The surface redshift is below the critical limit of 2, while the causality condition $0 \leq v_s^2 \leq 1$ and the adiabatic index $\Gamma > 4/3$ satisfy the key stability criteria. Together, these findings confirm the gravastar stable configuration within the $f(\mathcal{Q}, \mathbb{T})$ gravity framework.

Comparing with existing literature, our results align well with Sharif and Saba [68] in $f(\mathcal{G}, \mathbb{T}^2)$ gravity, where \mathcal{G} is the Gauss-Bonnet invariant, using the Finch-Skea metric with isotropic fluids, concluding their stability and physical plausibility. Faisal et al. [58] explored gravastar stability in $f(\mathcal{Q})$ gravity, finding consistent structural stability under various conditions. Our findings complement these studies, showcasing similar stability criteria while extending the analysis to the $f(\mathcal{Q}, \mathbb{T})$ framework. By integrating the

coupling between non-metricity and the energy-momentum tensor trace, our work provides new insights into gravastar properties, enhancing their theoretical foundation and broadening the scope of modified gravity theories. These results serve as a significant step forward in understanding gravastars and their role as viable, singularity-free alternatives to black holes. **Data Availability Statement:** No new data were generated or analyzed in support of this research.

References

- [1] Hubble, E.: Proc. Natl. Acad. Sci. U.S.A. **15**(1929)168.
- [2] Peebles, P.J.E. and Ratra, B.: Rev. Mod. Phys. **75**(2003)559.
- [3] Nester, J.M. and Yo, H.J.: Chin. J. Phys. **37**(1999)113.
- [4] Jimenez, J.B., Heisenberg, L. and Koivisto, T.: Phys. Rev. D **98**(2018)044048.
- [5] Adeel, M.: et al.: Mod. Phys. Lett. A **38**(2023)2350152.
- [6] Sharif, M.: et al.: Chin. J. Phys. **91**(2024)66.
- [7] Rani, S.: et al.: Int. J. Geom. Methods Mod. Phys. **21**(2024)2450033.
- [8] Gul, M.Z. et al.: Eur. Phys. J. C **84**(2024)8.
- [9] Maurya, S.K. et al.: Phys. Dark Universe **46**(2024)101619.
- [10] Sharif, M.: et al.: New Astron. **109**(2024)102211.
- [11] Rani, S.: et al.: Phys. Dark Universe **47**(2025)101754.
- [12] Sharif, M.: et al.: Phys. Dark Universe **47**(2025)101760.
- [13] Koussour, M. et al.: Phys. Dark Universe **46**(2024)101577.
- [14] Gul, M.Z. et al.: Chin. J. Phys. **88**(2024)388.
- [15] Sharif, M. et al.: Eur. Phys. J. C **84**(2024)1094.
- [16] Myrzakulov, Y. et al.: Phys. Dark Universe **45**(2024)101545.

- [17] Sharif, M. and Gul, M.Z.: *Ann. Phys.* **465**(2024)169674.
- [18] Errehymy, A. et al.: *Physics of the Dark Universe* **46**(2024)101555.
- [19] Sharif, M. and Gul, M.Z.: *Phys. Scr.* **99**(2024)065036.
- [20] Gul, M.Z. et al.: *Chin. J. Phys.* **89**(2024)1347.
- [21] Xu, Y. et al.: *Eur. Phys. J. C* **79**(2019)708.
- [22] Zhadyranova, A.: *J. High Energy Astrophys.* **44**(2024)123.
- [23] Gul, M.Z. et al.: *Phys. Scr.* **99**(2024)045006.
- [24] Koussour, M.: *Chin. J. Phys.* **90**(2024)108.
- [25] Sharif, M. et al.: *Phys. Scr.* **99**(2024)115003.
- [26] Gul, M.Z. et al.: *Chin. Phys. C.* **48**(2024)12503.
- [27] Koussour, M.: *Phys. Dark Universe* **45**(2024)101527.
- [28] Nan, G. et al.: *Phys. Dark Universe* **46**(2024)101635.
- [29] Gul, M.Z. et al.: *Eur. Phys. J. C* **84**(2024)802.
- [30] Sharif, M. et al.: *Mod. Phys. Lett. A* **39**(2024)2450140.
- [31] Pradhan, S. et al.: *Fortschr. der Phys.* **72**(2024)2400092.
- [32] Gul, M.Z. et al.: *Phys. Scr.* **99**(2024)045006.
- [33] Arora, S. et al.: *Phys. Dark Univ.* **30**(2020)100664.
- [34] Bhattacharjee, S. and Sahoo, P.K.: *Eur. Phys. J. C* **80**(2020)289.
- [35] Godani, N. and Samanta, G.C.: *Int. J. Geom. Methods Mod. Phys.* **18**(2021)2150134.
- [36] Agrawal, A.S. et al.: *Phys. Dark Univ.* **33**(2021)100863.
- [37] Shiravand, M., Fakhry, S. and Farhoudi, M.: *Phys. Dark Univ.* **37**(2022)101106.

- [38] Tayde, M., Hassan, Z. and Sahoo, P.K.: Phys. Dark Univ. **42**(2023)101288.
- [39] Sharif, M. and Ibrar, I.: Chin. J. Phys. **89**(2024)1578; Eur. Phys. J. Plus **139**(2024)1; Phys. Scr. **99**(2024)105034.
- [40] Mottola, E. and Mazur, P.O.: *Gravitational condensate stars: An alternative to black holes* (In APS April Meeting Abstracts, 2002); Mazur, P.O. and Mottola, E.: Proc. Natl. Acad. Sci. **101**(2004)9545.
- [41] Sakai, N. et al.: Phys. Rev. D **90**(2014)104013.
- [42] Kubo, T. and Sakai, N.: Phys. Rev. D **93**(2016)084051.
- [43] Mottola, E. and Mazur, P.O.: Universe **9**(2023)88.
- [44] Sotiriou, T.P. Visser, M. and Weinfurtner, S.: J. High Energy Phys. **9**(2023)88.
- [45] Cardoso, V., Franzin, E. and Pani, P.: Phys. Rev. Lett. **116**(2016)171101; **117**(2016)089902.
- [46] Akiyama, K. et al.: Astrophys. J. Lett. **875**(2019)L6.
- [47] Visser, M. and Wiltshire, D.L.: Class. Quantum Grav. **21**(2004)1135.
- [48] Carter, B.M.N.: Class. Quantum Grav. **22**(2005)4551.
- [49] Bilic, N. et al.: J. Cosmol. Astropart. Phys. **2006**(2006)13.
- [50] Ghosh, S. et al.: Results Phys. **14**(2009)102473.
- [51] Das, A. et al.: Phys. Rev. D **95**(2017)124011.
- [52] Shamir, M.F. and Ahmad, M.: Phys. Rev. D **97**(2018)104031.
- [53] Sharif, M. and Waseem, A.: Astrophys. Space Sci. **364**(2019)189.
- [54] Ghosh, S. et al.: Ann. Phys. **411**(2019)167968.
- [55] Bhatti, M.Z., Yousaf, Z. and Rehman, A.: Phys. Dark Univ. **29**(2020)100561.

- [56] Pradhan, S., Mohanty, D. and Sahoo, P.K.: Chin. Phys. C **47**(2023)095104.
- [57] Mohanty, D. and Sahoo, P.K.: Fortschr. Phys. **72**(2024)2400082.
- [58] Javed, F. et al.: Chin. J. Phys. **90**(2024)421.
- [59] Mohanty, D., Ghosh, S. and Sahoo, P.K.: Ann. Phys. **463**(2024)169636.
- [60] Odintsov, S.D. and Oikonomou, V.K.: Phys. Rev. D **107**(2023)104039.
- [61] Teruel, G.R.P. et al.: Phys. Dark Univ. **43**(2024)101404.
- [62] Sharif, M., Naseer, T. and Tabassum, A.: Chin. J. Phys. **92**(2024)579.
- [63] Dourah, H.L. and Ray, R.: Class. Quantum Grav. **4**(1987)1691.
- [64] Finch, M.R. and Skea, J.E.F.: Class. Quantum Grav. **6**(1989)467.
- [65] Bhar, P.: Astrophys. Space Sci. **359**(2015)41.
- [66] Paul, B.C. and Dey, S.: Astrophys. Space Sci. **363**(2018)220.
- [67] Banerjee, A., Jasim, M.K. and Pradhan, A.: Mod. Phys. Lett. A **35**(2020)2050071.
- [68] Sharif, M. and Naz, S.: Mod. Phys. Lett. A **38**(2023)2350123.
- [69] Dayanandan, B. et al.: Chin. J. Phys. **82**(2023)155.
- [70] Mustafa, G. et al.: Chin. J. Phys. **88**(2024)954.
- [71] Shahzad, M.R. et al.: Phys. Dark Univ. **46**(2024)101646.
- [72] Rej, P., Bogadi, R.S. and Govender, M.: Chin. J. Phys. **87**(2024)608.
- [73] Karmakar, A., Debnath, U. and Rej, P.: Chin. J. Phys. **90**(2024)1142.
- [74] Das, B. et al.: Astrophys. Space Sci. **369**(2024)76.
- [75] Weyl, H.: Sitzungsber. Preuss. Akad. Wiss. **465**(1918)01.
- [76] Dirac, P.A.M.: Proc. Math. Phys. Eng. Sci. **333**(1973)403.
- [77] Novello, M. and Bergliaffa, S.P.: Phys. Rep. **463**(2008)127.

- [78] Landau, L.D. and Lifshitz, E.M.: *The Classical Theory of Fields* (Elsevier, 2013).
- [79] Sharif, M. and Ajmal, M.: Chin. J. Phys. **88**(2024)706; Phys. Scr. **99**(2024)085039; Phys. Dark Univ. **46**(2024)101572.
- [80] Gul, M.Z., Sharif, M. and Arooj, A.: Fortschr. Phys. **72**(2024)2300221.
- [81] Gul, M.Z. et al.: Eur. Phys. J. C **84**(2024)775.
- [82] Gul, M.Z. et al.: Eur. Phys. J. C **84**(2024)1232.
- [83] Sharif, M. et al.: Phys. Scr. **99**(2024)115003.
- [84] Gul, M.Z. et al.: Gen. Relativ. Gravit. **56**(2024)45.
- [85] Sharif, M. et al.: Mod. Phys. Lett. A **39**(2024)2450140.
- [86] Gul, M.Z. et al.: Chin. J. Phys. **93**(2025)256.
- [87] Xu, Y. et al.: Eur Phys. J. C **79**(2019)19.
- [88] Xu, Y. et al.: Eur Phys. J. C **80**(2020)22; Tayde, M. et al.: Chin. Phys. C **46**(2022)115101.
- [89] Delgaty, M.S.R. and Lake, K.: Comput. Phys. Commun. **115**(1998)395.
- [90] Das, B. et al.: Eur. Phys. J. C **82**(2022)519; Murshid, M. et al.: Gen. Relativ. Grav. **97**(2023)51; Sokoliuk, O., Baransky, A. and Sahoo, P.K.: Chin. Phys. C **47**(2023)015104.
- [91] Deb, D. et al.: Ann. Phys. **387**(2017)239.
- [92] Ozel, F., Guver, T. and Psaltis, D.: Astrophys. J. **693**(2009)1775.
- [93] Zeldovich, Y.B.: Mon. Not. R. Astron. Soc. **160**(1972)1P.
- [94] Staelens, F. et al.: Gen. Relativ. Grav. **53**(2021)1.
- [95] Carr, J.B.: Astrophys. J. **201**(1975)1; Madsen, M.S. et al.: Phys. Rev. D **46**(1992)1399; Braje, T.M. et al.: Astrophys. J. **580**(2002)1043; Ferrari, L. et al.: Int. J. Mod. Phys. E **16**(2007)2834; Rahaman, F. et al.: Eur. Phys. J. C **74**(2014)2845.

- [96] Israel, W.: Nuo. Cim. B **44**(1966)1.
- [97] Sen, N.: Ann. Phys. **378**(1924)365.
- [98] Darmois, G. et al.: *Memorial des sciences mathematiques* (Gauthier-Villars Paris, 1927).
- [99] Israel, W.: Nuo. Cim. B **48**(1967)463.
- [100] Sharif, M. and Javed, F.: Eur. Phys. J. C **81**(2021)1.
- [101] Mustafa, G. et al.: Phys. Dark Univ. **46**(2020)101574.
- [102] Ghosh, S. et al.: Phys. Lett. B **767**(2017)380.
- [103] Buchdahl, H.A.: Phys. Rev. **116**(1959)1027; Barraco, D.E. and Hamity, V.H.: Phys. Rev. D **65**(2002)124028.
- [104] Chandrasekhar, S.: Astrophys. J. **140**(1964)417; Chan, R., Herrera, L. and Santos, N.: Mon. Not. R. Astron. Soc. **265**(1993)533.
- [105] Poisson, E. and Visser, M.: Phys. Rev. D **52**(1995)7318.
- [106] Lobo, F.S.N. and Crawford, P.: Class. Quantum Grav. **21**(2003)391.
- [107] Sharif, M. and Saeed, M.: Chin. J. Phys. **77**(2022)583.
- [108] Das, A. et al.: Nucl. Phys. B **954**(2020)114986.
- [109] Shah, H. et al.: Phys. Scr. **98**(2023)085246.